Surface Morphology of Annealed Polystyrene and Poly(methyl methacrylate) Thin Film Blends and Bilayers

Mark Harris, Guenter Appel, and Harald Ade*

Department of Physics, North Carolina State University, Raleigh, North Carolina 27695

Received October 1, 2002

ABSTRACT: Thin films of polystyrene (PS) and poly(methyl methacrylate) (PMMA) were spun-cast onto silicon substrates, annealed, and analyzed by atomic force microscopy (AFM), total electron yield (TEY), and partial electron yield (PEY) near-edge X-ray absorption fine structure (NEXAFS) spectroscopy in order to resolve conflicting prior literature regarding the tendency of PS to form a wetting layer or overlayer on top of PMMA. From the comparison of the three methods of analysis and on the basis of the extraordinary surface sensitivity of PEY NEXAFS, we conclude that PS does not form an overlayer in samples with morphologies near thermodynamic equilibrium. The PS forms droplets of a large size range on top of a PMMA layer that wets the hydrophilic SiO_x substrate. From our results, the maximum thickness of a continuous PS wetting layer would be about 0.25 nm. This is in contrast to recent experiments that imply an equivalent PS wetting layer of about 5−10 nm is forming during annealing.

Introduction

Polystyrene (PS) and poly(methyl methacrylate) (PMMA) are frequently used as binary model systems to study thin film polymer structure formation, polymer−polymer and polymer−substrate interactions, and pattern formation and phase separation dynamics in polymer thin films.[1−7] In most cases, the results observed in annealed PS/PMMA systems are consistent with or where interpreted as phase-separated films without any wetting layer at the air interface, i.e., a situation in which neither polymer wets the other. Walheim et al. reported droplets of PS after annealing a 50/50 w/w sample for 12 h at 190 °C.[3] Ade et al. have also found surface phase-separated PS and PMMA domains with PS droplets after annealing at 180 °C.[2] If other morphologies were found for the same weight ratio, either the samples were not annealed[1] or a different substrate was used.[3] In contrast, results with PS/PVME[8] and PS/PBrS[9−11] systems clearly indicated wetting layers of PS over PVME and PBrS, respectively, due to different interfacial and surface energies in these systems.

In contrast to the interpretation in prior investigations of PS/PMMA systems, recent investigations reported the formation of a PS overlayer during annealing of a PS/PMMA thin film polymer blend at 142 °C. On the basis of angle-resolved X-ray photoelectron spectroscopy (XPS) and friction force microscopy, Ton-That et al. concluded to find a PS overlayer,[12] implying that this is the thermodynamically favored morphology. The measured PMMA concentration of only 9% at an electron takeoff angle of 60°, corresponding to the most surface-sensitive measurement with a depth sensitivity of 4.5 nm, would imply an equivalent PS wetting layer of about 10 nm.

On the basis of thermodynamic equilibrium considerations, one would expect annealed PS and PMMA blends to be phase-separated in the bulk, but also right to the surface. For example, the surface tensions of 3K PMMA and 44K PS are $\gamma_{PMMA} = 41.1$ mJ/m^2 and $\gamma_{PS} = 40.7$ mJ/m^2 at 20 °C, while $\gamma_{PMMA} = 32.0$ mJ/m^2 and $\gamma_{PS} = 32.1$ mJ/m^2 at 140 °C. The interfacial tension between these two materials is 3.2 mJ/m^2 at 20 °C and 1.7 mJ/m^2 at 140 °C.[13] Since the surface tensions, γ, of pure PS and pure PMMA are very similar at typical annealing temperatures, the interfacial energy $\gamma_{PS/PMMA}$ is the driving force in determining the surface morphology. For typical annealing temperatures, the interfacial tension $\gamma_{PS/PMMA}$ is larger than the absolute value of the surface tension difference, so the spreading parameters for PS spreading on PMMA, $S_{PS} = \gamma_{PMMA} - \gamma_{PS} - \gamma_{PS/PMMA} = -1.8$ mJ/m^2, and for PMMA spreading on PS, $S_{PMMA} = \gamma_{PS} - \gamma_{PMMA} - \gamma_{PS/PMMA} = -1.6$ mJ/m^2, are both negative at 140 °C. The spreading parameters decrease for higher temperatures, but both remain negative for temperatures <220 °C. Thus, neither polymer should wet the other for typical annealing temperatures. The interfacial area, rather than the surface area of a specific polymer, is expected to be minimized as much as possible. The wetting behavior at the substrate interface depends on the substrate utilized. On a relatively hydrophilic surface such as a clean, native Si oxide or mica, the more polar PMMA is strongly attracted to the substrate interface and forms a wetting layer upon annealing. Overall, on a hydrophilic substrate, one would expect PS droplet formation on top of a PMMA substrate wetting layer. Hence, PS would form droplets and PMMA would form the "matrix" for a range of PS/PMMA compositions and starting morphologies as the samples evolve toward the thermodynamic equilibrium during annealing.

Because of the frequent use of PS and PMMA in polymer thin film experiments and their potential use as surfaces to study preferential adsorption of molecules and particles, the conflict in the literature regarding a PS wetting layer needs to be resolved. To provide clarification, PS/PMMA thin film blends and bilayers were prepared by spin-casting. They were subsequently annealed at 170 °C in a vacuum oven and analyzed using methods that provide complementary information: atomic force microscopy (AFM), total electron yield (TEY), and partial electron yield (PEY) near-edge X-ray absorption fine structure (NEXAFS) spectroscopy.[14]

* Corresponding author: e-mail harald_ade@ncsu.edu; phone 919-515-1331; fax 919-515-4496.

10.1021/ma0257043 CCC: $25.00
Published on Web 04/10/2003

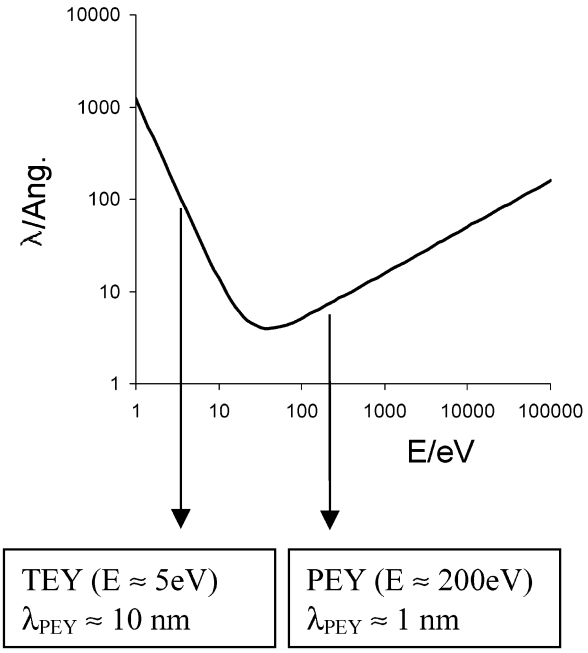

Figure 1. Schematic of mean free path λ of electrons in solids as a function of their kinetic energy. The arrows mark the approximate average energies of the electrons used for TEY and PEY NEXAFS.

In NEXAFS, the transition energy is governed by core and antibonding states. Hence, the characteristic signals of PS and PMMA are much more clearly separated from each other as well as from other polymers or carbonaceous contaminants than in XPS spectra.[14] In addition, the C 1s $\rightarrow \pi^*$ transition corresponding to the phenyl and carbonyl moieties have sharper, and hence more intense, spectral features on a per carbon atom basis than the C 1s $\rightarrow \sigma^*$ transitions of C−C and C−H bonds. This results in excellent compositional sensitivity for PS and yields good quantitation for both polymers. In contrast, XPS exhibits only a small shake-up feature as a direct signature of PS. Furthermore, the information depth can be tuned in NEXAFS by choosing the energy of the electrons accepted for the spectral signal. Figure 1 schematically shows the electron mean free paths in solids vs their kinetic energy, the so-called universal curve.[15] For TEY NEXAFS, slow secondary electrons of about 5 eV dominate the signal. In contrast, PEY NEXAFS with a retarding voltage of typically 150 V only accepts Auger electrons and scattered electrons with an average energy of about 200 eV. This results in a mean free path or sampling depth of about 1 nm for PEY NEXAFS and about 10 nm for TEY NEXAFS. Thus, in addition to the improved spectral sensitivity to PS, the sampling depth of PEY NEXAFS spectroscopy is about an order of magnitude smaller than that of XPS with a laboratory X-ray source and about a factor 5 better than the sampling depth of XPS under electron takeoff angle of about 60°. Since the information depth of PEY NEXAFS is less than the radius of gyration of the PS utilized (4.0 nm for a molecular weight of 21 000 g/mol,[16]) a continuous wetting layer of PS on top of PMMA should result in a readily detectable NEXAFS spectrum corresponding to almost pure PS. We estimate the smallest detectable surface fraction of PS to be <5% PS, equivalent in PEY NEXAFS to a layer of about 0.05 nm.

Electron yield NEXAFS spectroscopy typically averages over several square millimeters of the sample surface to a depth in the range of the values mentioned above. In contrast, AFM probes the very surface morphology at high spatial resolution but provides no chemical information. By comparing AFM images of as-annealed samples to AFM images of differentially washed samples, structural models can be developed[1−3] that allow the identification of certain features in the AFM images (droplets) with a polymer component (PS). Using such information, a quantitative evaluation of AFM images from as-annealed samples yields surface compositional information, which can be compared with the composition and structural models derived from NEXAFS spectra. We will show that PS and PMMA form separate domains at the surface without any appreciable PS overlayer on top of PMMA.

Table 1. Description of Bilayer Samples

molecular weight, M_w, g/mol	concentration of solutions, mg/mL	thickness, nm
	PS Layer (Top)	
20 870	15.0	67 ± 6
	PMMA Layer (Bottom)	
21 530	15.6	54 ± 6
21 530	26.1	102 ± 7
100 300	3.5	17 ± 5
100 300	15.6	68 ± 6
100 300	26.1	119 ± 13

Experimental Section

The substrates utilized were approximately 2 cm^2 pieces of Si(100) wafers with a natural oxide. Dust and other particles were removed from the substrates with compressed nitrogen, and the silicon was then further cleaned with water, methanol, and chloroform. After this treatment the substrates had a water contact angle of 26°.

The polymers were dissolved in toluene to concentrations ranging from 3.5 to 26.1 mg/mL, filtered to remove undissolved particles, and then spun-cast onto the freshly cleaned silicon substrates at 2100 rpm for 30 s. Three types of samples were prepared: blends of varying composition cast from mixtures of PS and PMMA in a common solvent, PS/PMMA bilayers with PS on top of PMMA, and pure PS and PMMA reference films. The primary variables in the process of preparing the sample sets were the following:

• Molecular weight of the polymers. Monodisperse PS with molecular weight of M_w = 104 000 g/mol (polydispersity index (PD) = 1.05, from Polymer Source), PS of M_w = 20 870 g/mol (PD = 1.02, Polymer Laboratories), and PMMA with M_w = 100 300 g/mol (PD = 1.04) and 21 530 g/mol (PD = 1.03) were utilized (all PMMA materials from Polymer Laboratories). For simplicity, these materials are in the following referred to as PS_{104}, PS_{21}, $PMMA_{100}$, and $PMMA_{22}$, respectively. Blends were made from PS_{21} and $PMMA_{22}$, with the exception of the 50/50 PS/PMMA samples spun from chloroform solutions, which used PS_{104} and $PMMA_{100}$ instead. Pure PMMA reference samples for NEXAFS investigations were made of $PMMA_{100}$. Bilayers with both $PMMA_{100}$ and $PMMA_{22}$ were produced (see summary in Table 1).

• Weight by weight ratio of PS to PMMA. In the bilayers of PS on top of PMMA, the molecular weight and the thickness of the PMMA layer were varied. PS/PMMA blends where prepared with mass ratios in solution of 70/30, 50/50, 30/70, and 10/90 PS to PMMA.

• Concentration of the solution. The total polymer concentration for the blends was 25.8 mg/mL. Concentration for the PS layer of the bilayers was 15 mg/mL. The PMMA layer was varied in thickness by using different concentrations (Table 1). PS reference samples for thickness measurements were prepared from 25.8 mg/mL solutions of PS_{21}.

• Tacticity of PMMA. In contrast to PS, where the tacticity has almost no influence on properties like the glass transition temperature T_g, the tacticity has a substantial effect on T_g of

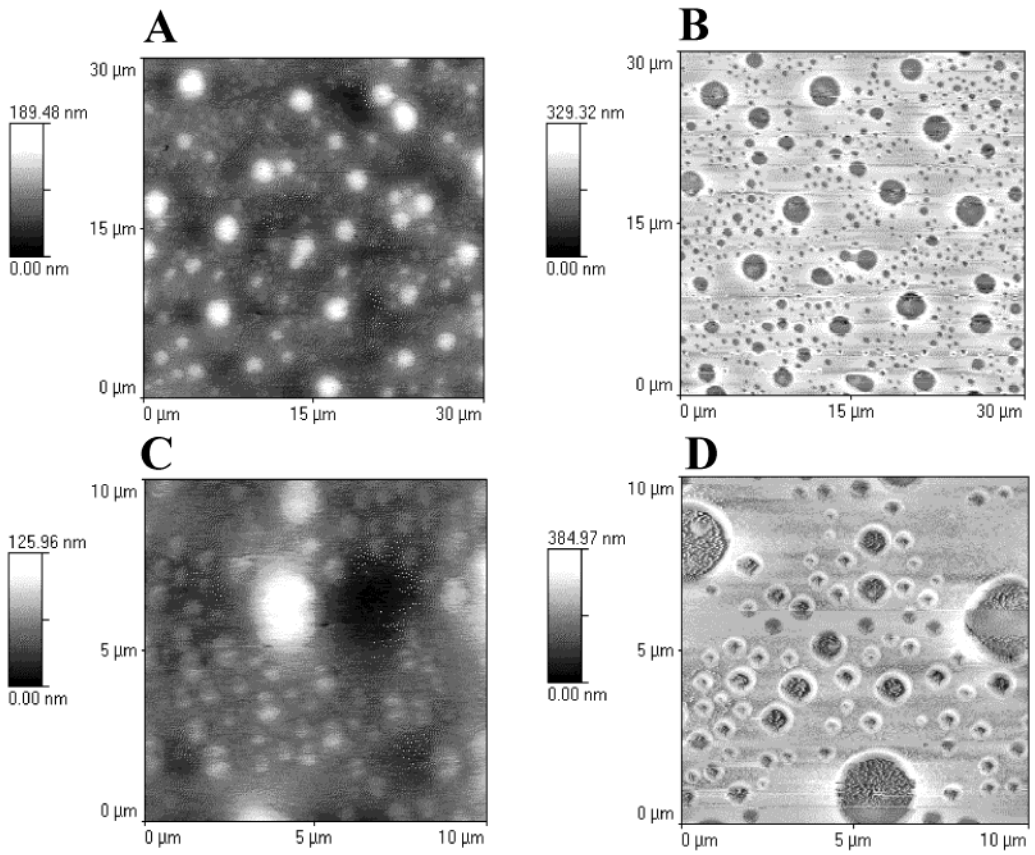

Figure 2. AFM images of a 30/70 $PS_{21}/PMMA_{22}$ blend annealed for 2 days at 170 °C before and after washing with cyclohexane: (A) 30 μm by 30 μm image before washing and (B) after washing; (C) 10 μm by 10 μm image before washing and (D) after washing.

PMMA.[17] The $PMMA_{22}$ was 16.5% isotactic, 80% syndiotactic, and 3.5% atactic. The $PMMA_{100}$ material was 35−45% isotactic, 50−60% syndiotactic, and 5% atactic. Thus, the T_g of $PMMA_{100}$ would be 103 °C and somewhat lower for $PMMA_{22}$.

• Solvent. Differences in solubility of PS and PMMA in different solvents and differences in the viscosity influence the initial morphology after spin-coating. Nevertheless, the solvent used for casting should have little effect on the morphology at or close to the thermodynamic equilibrium of the polymer samples. We used toluene for casting, except for the 50/50 $PS_{104}/PMMA_{100}$ samples which were cast from chloroform solution.

• Annealing temperature and times: The samples were annealed at 170 ± 2 °C in a vacuum oven. The annealing time ranged from 2 to 8 days for the 50/50 $PS_{104}/PMMA_{100}$ blend cast from chloroform. All other samples were annealed for 2 days. A temperature of 170 °C is well above the glass transition temperature of the polymers (ca. 95 °C for PS,[17] PMMA see above). Some samples were left unannealed, usually for the purpose of measuring the sample thickness.

To make the bilayers, a PMMA layer was spun-cast and annealed for 1 day at 170 °C; subsequently, a PS layer was spun-cast directly on top of the PMMA. Differential solvent washing with cyclohexane was used on annealed samples to confirm the PMMA layer remains unperturbed. The bilayer samples were annealed for 2 days at 170 °C.

A Thermomicroscopes Autoprobe CP Research AFM was used in contact mode to characterize the surface topography and in lateral force mode in an attempt to characterize the surface composition. The TM microscopes software was used to perform a quadratic background subtraction. Since the lateral force images consistently exhibited artifacts associated with topography, the commonly used practice of differentially dissolving one of the polymers[1−3,7] was used to test whether particular morphological features observed with the AFM were PS or PMMA. A 30/70 $PS_{21}/PMMA_{22}$ and a 50/50 $PS_{104}/PMMA_{100}$ blend sample were washed with cyclohexane for approximately 30 s to dissolve the PS and to leave the PMMA. Film thicknesses of unannealed samples were measured with the AFM. The films were scratched lightly with sharp tweezers, and the thickness was characterized by averaging AFM line profiles perpendicular to the scratch direction.

To determine the average surface composition, NEXAFS experiments were performed at beamline U4B at the National Synchrotron Light Source (NSLS). The samples were mounted on a sample paddle and were heated for several hours under vacuum to temperatures less than 60 °C during a mild bake-out. TEY NEXAFS measurements were conducted by measuring the sample current from the electrically isolated sample paddle. A channeltron was used for PEY NEXAFS spectra. Slow electrons were rejected from reaching this detector by applying a voltage of −150 V at the front end of the channeltron funnel. The energy step size of the spectra was 0.1 eV in the region between 280 and 310 eV and 0.5 eV below and above this interval (260−280 and 310−350 eV). To normalize out fluctuations in X-ray intensity as well as to correct for some of the systematic changes in incident intensity with photon energy, the signal from a gold mesh was measured simultaneously with the sample current or the channeltron signal, respectively. Reference spectra of pure PS and PMMA samples were measured under the same conditions.

Results

The layer thickness of the polymer films was determined by averaging the AFM line profiles perpendicular to the scratch direction within a rectangular area and by averaging the height differences between the undisturbed film and the bottom of the scratch from several of these areas. Table 1 shows the thicknesses of the PMMA films used as the bottom layer of the bilayers. The total thickness of a $PMMA_{100}$ (3.5 mg/mL)−PS_{21} (15 mg/mL) bilayer was determined to be 84 ± 3 nm. Subsequently, the PS layer was washed off with cyclo-

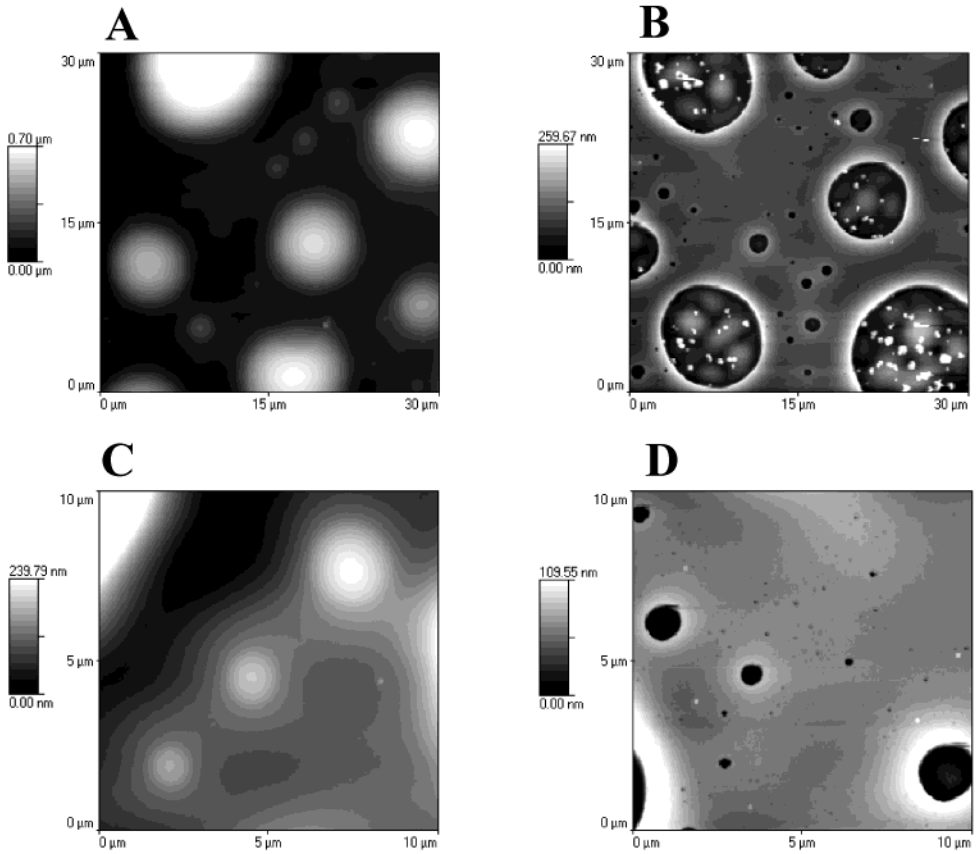

Figure 3. AFM images of a 50/50 $PS_{104}/PMMA_{100}$ blend annealed for 8 days at 170 °C before and after washing with cyclohexane: (A) 30 μm by 30 μm image before washing and (B) after washing; (C) 10 μm by 10 μm image before washing and (D) after washing.

hexane and the remaining layer scratched again. Although the film was rougher than before this treatment, the original PMMA film thickness of 17 nm was preserved. Thus, the PMMA is not dissolved or washed away during the spin-coating of the PS on top of the PMMA layer, and the PS layer thickness of the unannealed bilayer is 67 ± 6 nm.

The PS_{21} (25.8 mg/mL), 50/50 $PS_{21}/PMMA_{22}$ (25.8 mg/mL), and $PMMA_{22}$ (26.1 mg/mL) samples had measured thicknesses of 98 ± 3, 99 ± 9, and 102 ± 7 nm, respectively. On the basis of this consistency, we subsequently assumed that the thickness of all $PS_{21}/PMMA_{22}$ blends samples was 100 ± 6 nm. For the 50/50 $PS_{104}/PMMA_{100}$ sample spun from chloroform, a thickness of 220 ± 20 nm was determined.

AFM topography images were acquired from all samples. Figure 2 shows images of an annealed 30/70 $PS_{21}/PMMA_{22}$ blend before and after washing with cyclohexane. Figure 2A is a 30 μm by 30 μm image before washing. Figure 2B is an image of the same size after preferential washing. Figures 2C and 1D show 10 μm by 10 μm images of the same sample before and after washing, respectively. Figure 3 shows analogous images for an annealed 50/50 $PS_{104}/PMMA_{100}$ sample cast from chloroform. Generally, images of the as-annealed samples show a series of droplets of varying sizes, whereas images acquired after cyclohexane washing exhibit holes of the same size distribution and frequency. This clearly indicates that the droplets observed in topography AFM are composed of PS, and the matrix is PMMA. We note that particularly the small holes are discerned much more clearly in the washed samples than the corresponding droplets in AFM topography images. This indicates that the majority of the material in small PS domains is beneath the surface level of the PMMA matrix or below the small PMMA rim that accompanies each PS domain that cannot sink deep enough into the PMMA matrix due to the finite sample thickness and the constraint to have a PMMA wetting layer on the SiO_x substrate interface. These morphologies are a result of the balancing of surface and interfacial tensions in a liquid−liquid system, when the surface tensions of the two components are nearly equal and the Neuman angle has to be considered.[18] The larger PS droplets cannot sink deep enough into the PMMA matrix due to the substrate and cannot fulfill the Neuman angle condition without pulling up the contact line with the PMMA, thus resulting in a rim of PMMA. The PMMA rim that accompanies large surface-segregated PS domains and the extension of small PS domains into the PMMA layer results in features of high gradients, contributing to the higher visibility of the PS domains in the cyclohexane-washed samples.

Figures 2−4 show examples of AFM topography images of several as-annealed samples. Figure 2A shows droplets of the 30/70 $PS_{21}/PMMA_{22}$ blend. Figure 2C shows a smaller region of the same sample, which reveals smaller droplets between the larger ones. (The very small, semiperiodic features in dark areas in several of the images, e.g., in Figure 2C,D, are noise artifacts and not features of the sample.) Figure 3A,C shows images of a 50/50 $PS_{104}/PMMA_{100}$ blend spun from a chloroform solution. These images reveal that this sample also exhibits PS droplets with a large size distribution. Figure 4 shows images of an annealed bilayer with a PS top layer on a thin layer of high

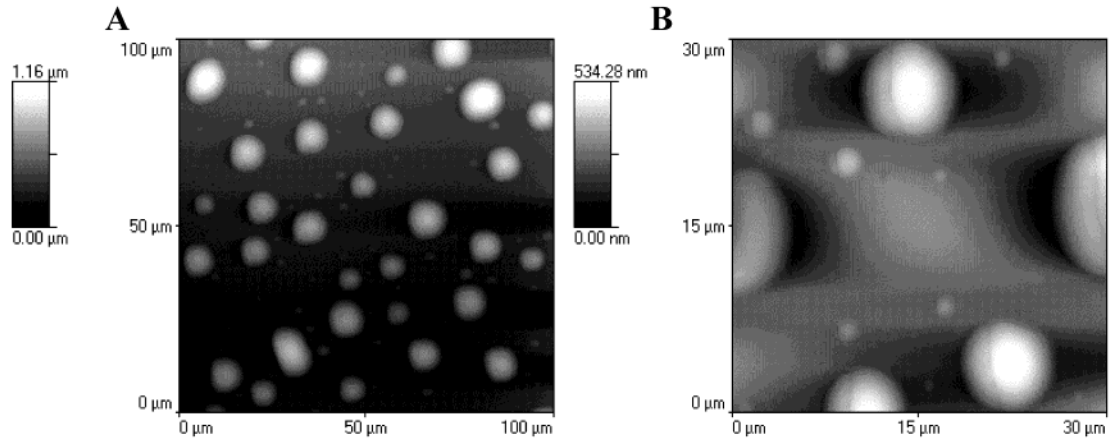

Figure 4. AFM images of a bilayer of 67 nm PS_{21} on top of 17 nm $PMMA_{100}$ annealed for 2 days at 170 °C: (A) 100 μm by 100 μm; (B) 30 μm by 30 μm. The dark areas left and right of some elevated structures are artifacts introduced by the (line-by-line) least-squares algorithm of the background subtraction.

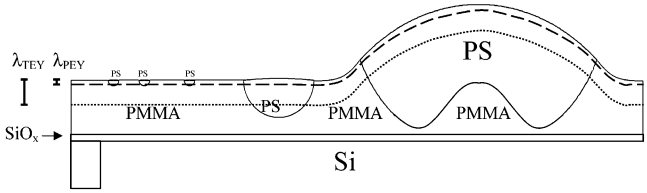

Figure 5. Schematic (not to scale) of PS/PMMA blends and PS on PMMA bilayers after annealing. In the right part a large PS droplet that reaches the substrate and cannot sink sufficiently deep and its surrounding PMMA rim is represented. PMMA is trapped underneath. The sampling depths of TEY and PEY NEXAFS, λ_{TEY} and λ_{PEY}, and their relationship to PS domains of different sizes are shown to the left.

molecular weight $PMMA_{100}$. Note that the morphologies of the samples of Figures 3 and 4 are very similar to each other and also similar to that of Figure 2, except that the droplets are much larger in Figure 4.

All samples investigated with AFM were found to be covered with droplets of varying size and with typically a bimodal, sometimes even a trimodal, size distribution. On the basis of the preference of the PMMA for the SiO_x substrate, considerations of the wetting parameters, and the results of selective cyclohexane washing, the droplets represent PS domains on top of a PMMA matrix or PMMA substrate wetting layer. Figure 5 shows a schematic representation of this morphology. Droplet-shaped PS domains of different sizes can be found on top of a PMMA layer. If the PS droplets are very large, PMMA can be trapped underneath, resulting in a relatively complicated interface (Figure 3B).[2] The NEXAFS results discussed below confirm a morphological model that is characterized by an absence of a PS wetting layer.

To estimate the surface area fraction of the PS droplets from the AFM topographs, we determined the bearing ratio. This provides the area percentage of features above a certain height, chosen to be just above the apparent transition from the matrix to most of the droplets. Figure 6 shows an example of this process. The large range in size of the droplets, errors resulting from the instrument background and its imperfect correction by a quadratic function, and the PMMA rim for large droplets resulted in systematic underestimating the PS surface fraction as some small droplets were not properly accounted for. The results as determined by the bearing ratio procedure are thus estimates of the minimum fractional surface area covered by PS. They are summarized in Table 2.

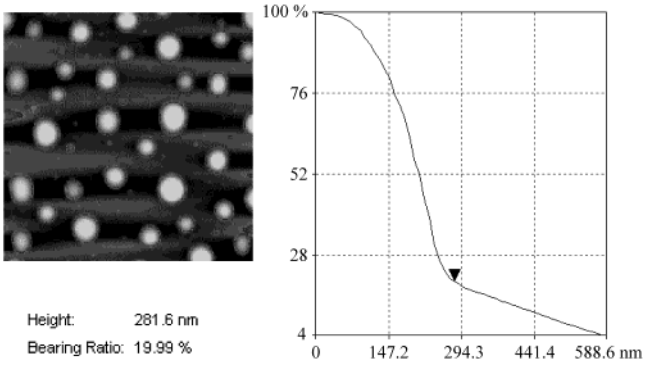

Figure 6. Bearing ratio evaluation of an AFM image of the annealed 70/30 $PS_{21}/PMMA_{22}$ blend The graph displays height on the horizontal axis and percentage of the sample surface above that height on the vertical axis. The marker on the graph shows the selected height, and the round, uniform, light gray areas in the image correspond to portions of the sample surface that are above that height.

Table 2. Sample Composition and Surface Fraction of PS from AFM Bearing Ratio Evaluation

Blends		
wt % PS in toluene solution	mol wt of polymers PS/PMMA, g/mol	% PS from AFM analysis
10	21K/22K	15
30	21K/22K	42
50	21K/22K	12
70	21K/22K	24
50	104K/100K	31
Bilayers		
thickness of PMMA layer, nm	PMMA mol wt, g/mol	% PS from AFM analysis
54 ± 6	22K	24
102 ± 7	22K	23
17 ± 5	100K	16
68 ± 6	100K	18
119 ± 13	100K	16

All NEXAFS spectra were normalized to the signal of the gold mesh and additionally normalized to a step height of unity between 283 and 315 eV. As reference spectra for the analysis of all blends and bilayer samples, TEY spectra of pure PS and PMMA samples were used. These TEY spectra are less affected than

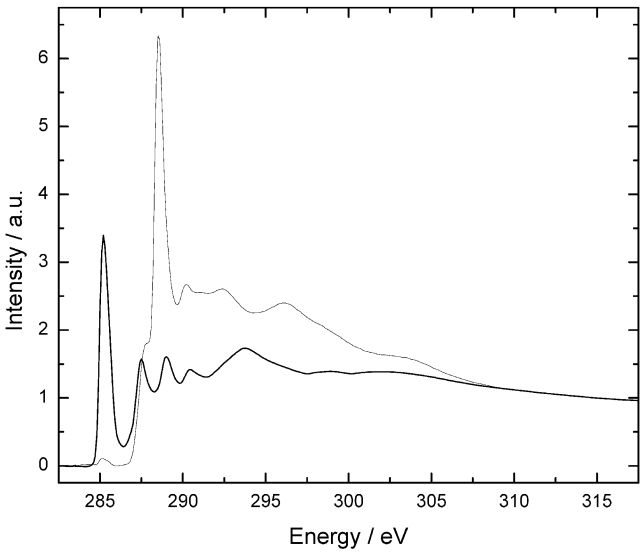

Figure 7. TEY-NEXAFS spectra of PS (thick line) and PMMA (thin line) used as reference spectra for the determination of the PS surface fraction of the blend and annealed bilayer samples. The spectra are normalized to a step height of unity between 283 and 315 eV.

PEY by potential surface contaminants or (unlikely) orientation effects of functional groups near the surface. To account for small experimental energy shifts and changes in linearity between spectra, the energy difference between the PS C 1s $\rightarrow \pi^*_{C=C}$ and the PMMA C 1s $\rightarrow \pi^*_{C=O}$ peaks was measured for all samples, and differences of 3.34 and 3.29 eV were established for the TEY and PEY spectra, respectively. The NEXAFS spectra presented here have a slightly different shape and intensity than previously reported NEXAFS spectra of PS and PMMA.[2,19,20] This is a reflection of the particular beamline and gold mesh normalization characteristics. Since all spectra used for the compositional analysis in this paper, including the reference spectra, were acquired under identical conditions, we have an internally consistent data set which will yield the correct sample composition. For the fit procedure the reference spectra were shifted in such a way that the PS π^* peaks of sample and reference spectra occurred at the same energy and the π^* of the PMMA reference at energies 3.34 eV (TEY) and 3.29 eV (PEY) higher. Figure 7 shows the reference spectra in the relative energy position for the evaluation of TEY spectra. To determine the average surface PS fraction of the blend and annealed bilayer samples, the experimental spectra were fit by a linear combination of the PS and PMMA reference spectra and a linear background. Because PMMA has no spectral features in the energy region below 287 eV, the weight of the PS component can easily be found by fitting the intensity of the PS π^* peaks of the sample and the reference spectrum. The weight of the PMMA spectrum and the slope of the background can then be determined by a least-squares method with the side condition that the intensities of the component spectra (I_{PS} and I_{PMMA}) and the linear background add up to unity at 315 eV.

As an example for the NEXAFS compositional analysis, Figure 8 shows the experimental TEY spectrum, the simulated spectrum, and the difference between the experimental and the simulated spectrum of the annealed bilayer (PMMA layer thickness of 17 nm prepared from $PMMA_{100}$). The small residual error and the nature of the residual "spectrum" indicate that there was very little carbonaceous surface contamination.

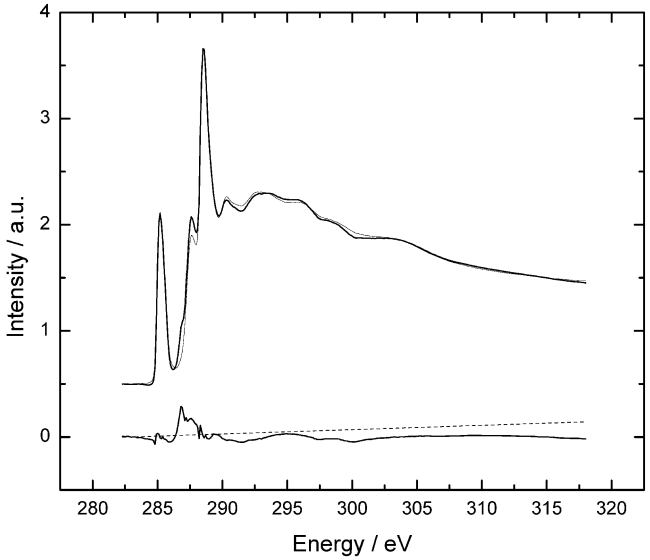

Figure 8. Experimental TEY-NEXAFS spectrum (thick solid line), simulated spectrum (a linear combination of the reference spectra and a linear background, thin solid line), residual spectrum (difference between experimental and simulated spectrum, gray solid line), and linear background (dashed line) for a bilayer of 67 nm PS_{21} on top of 17 nm $PMMA_{100}$ annealed for 2 days at 170 °C. Experimental and simulated spectra are both shifted by 0.5 intensity units for clarity. The deduced composition is 45% PS and 55% PMMA.

Since the only carbon in the sample is in the form of PS and PMMA, the percentage of PS of all carbon atoms %C_PS is given by

$$\%\text{C\_PS} = \frac{I_{PS}}{I_{PS} + I_{PMMA}} \times 100$$

Considering the differences in stoichiometry and density between PS and PMMA % PS, the volume fraction of PS within the sampling depth of NEXAFS can be easily determined from %C_PS. Figure 9 shows the resulting volume fractions of PS, which is equivalent to the fractional surface area coverage if the domains span the sampling depth. These results establish an upper bound for the thickness of a continuous PS layer to be discussed below. The results of AFM, TEY, and PEY are compared in Figure 9.

Discussion

The methods used to characterize the samples have strengths and weaknesses that complement each other. AFM is very sensitive to the surface topography, but the position of the borders of the droplets is unclear because there is a smooth transition from the PMMA to the PS domains. AFM is also unable to detect very shallow droplets in the presence of large droplets. If clear frictional images could be achieved similar to prior results,[2] they tended to be too noisy and too much affected by the topography to be used for quantitative compositional analysis. The images of the samples washed with cyclohexane clearly indicate that the sample matrix consists of PMMA, and that the droplets are PS. Even the 70/30 $PS_{21}/PMMA_{22}$ blend (Figure 6) formed the same droplet morphology and yielded relatively little surface area coverage as the majority of the PS was condensed into large, thick, and thus high volume droplets with a large volume/surface ratio. The larger PS drops were consistently several hundred

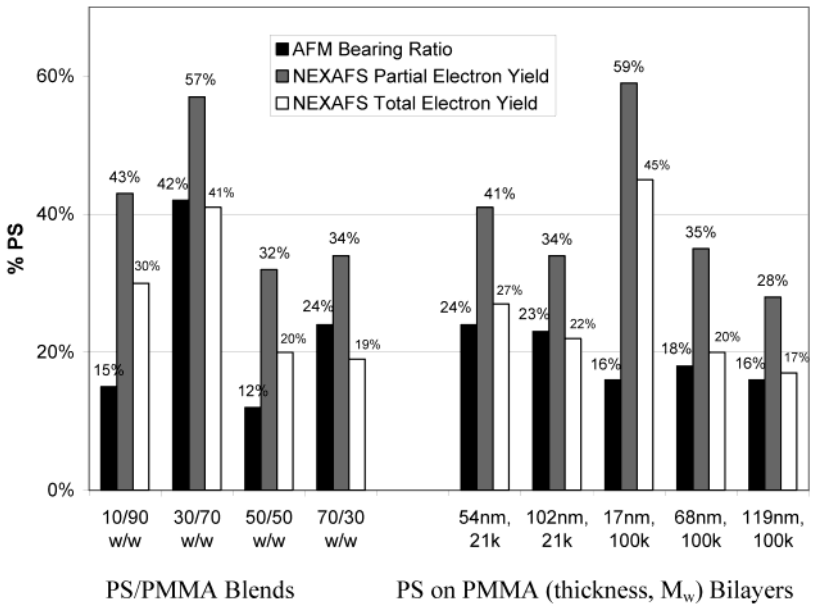

Figure 9. Graphical representation of the derived fractional surface area coverage (AFM) and the volume fraction of PS at the surface (PEY and TEY NEXAFS) for samples annealed at 170 °C.

nanometers nm in height, indicating considerable roughening of the initially about 100 nm thick samples. Even though the observed morphology, including the PMMA rims that hug the larger PS droplets, is strongly indicative that there is no PS wetting layer, it does not directly, i.e., based on measurements, exclude a very thin, relatively uniform layer of PS that could have been on top of the PMMA matrix prior to cyclohexane washing. It is for this reason that the NEXAFS experiments were performed.

All our data yield a surface composition of significantly less than 60% PS for each of the three methods. The averages of all samples of 21%, 27%, and 40% for AFM, TEY, and PEY, respectively, are significantly smaller than 50%. The PS fraction from AFM is similar to or smaller than that observed with TEY and smaller than PEY NEXAFS. This result is due to very small PS droplets that were detected by PEY NEXAFS and not by AFM, since droplets of height less than a nanometer above the matrix can usually not be seen between droplets of over a micrometer in height. Comparison of the PEY NEXAFS and TEY NEXAFS data also shows that PS is more abundant near the surface than it is throughout the TEY NEXAFS sampling depth of about 10 nm. This is a reflection of the small and, hence, shallow and thin droplets of PS at the PMMA surface that can be observed in the cyclohexane-washed samples. These results are illustrated in Figure 5: Very shallow PS droplets have a considerable influence only in the PEY signal, while the TEY averages over a much thicker layer of the sample that contains more PMMA. Overall, there is good correlation between the AFM bearing ratio and the PS fractions determined with NEXAFS, with the bearing ratio consistently underestimating the PS fraction due to the above-mentioned reason for missing the smallest droplets.

On the basis of the three methods of analysis utilized, we conclude that PS does not form an overlayer, but rather forms droplets with a large size distribution on top of a PMMA layer. This can be most appreciated by estimating an upper layer thickness that a continuous PS layer outside the PS droplets would have to have in order to explain the NEXAFS and AFM data consistently. The previous upper bound deduced from transmission NEXAFS microscopy had established an upper limit of 1 nm for a PS wetting layer.[21] Because of the inherent small sampling depth of PEY NEXAFS of 1 nm, the precision of this upper bound can be greatly improved. The PEY data of all samples yield an average surface composition of about 40% PS. The average minimum PS droplet surface fractional coverage from AFM analysis is 21%. If the excess PS signal, 19%, were to be evenly distributed over the remaining 79% of the surface, an equivalent thickness for a continuous PS layer of approximately (1 nm) × 19%/79% = 0.24 nm would result. At best, this corresponds to a few isolated PS molecules on the surface. These compositional results and the AFM images are most consistently explained with dispersed, small PS droplets on top of a pure PMMA matrix in the presence of a few large PS droplets.

Our results clearly indicate that there is no thermodynamic driving force for PS to form even a very thin, quasi-continuous PS wetting layer, from which the PS might autophobically dewett into PS droplets.[22] The PEY NEXAFS signal is simply too small to suggest that, and the morphological models deduced from washed AFM samples support this conclusion. The surface enrichment of PS upon annealing in the PS/PMMA samples of Ton-That et al. remains to be explained. We offer the following possible explanation. Ton-That et al. started from a structure predominantly consisting of a PMMA overlayer on a PS layer as a result of spinning from a chloroform solution. This is a starting morphology much further from the thermodynamic equilibrium than the starting morphologies in toluene-cast samples, consisting of blends that start out phase-separated in the spun-cast state as well as bilayers with the PS on top of PMMA. Furthermore, Ton-That et al. used higher or similar molecular weight PS and higher and similar molecular weight PMMA compared to us as well as lower and shorter annealing temperatures (42 h at 142 °C vs up to 8 days at 170 °C). Hence, our samples evolved more rapidly and closer toward thermodynamic equilibrium than those of Ton-That et al. The morphologies observed and described by Ton-That et al. are

rather different than those described here. From a theoretical perspective, there should not be, near thermodynamic equilibrium, the kind of surface topography and sample morphology proposed by Ton-That et al., even if there is a preference to establish a PS wetting layer. If we conjecture PS on top of PMMA and the well-established PMMA wetting layer on the substrate, a PS/PMMA bilayer should result, or the PS might form a very thin surface/interface layer of PS from which the PS autophobically dewetts to form droplets.[22] The PMMA itself would evolve toward a nearly uniform layer in order to minimize the interfacial area with the PS. The film should be either flat or roughen into droplets but should not have the PS hole morphology proposed by Ton-That et al.

In support of their observation, Ton-That et al. used the spreading parameter S to argue that the initial PMMA layer on top of a predominantly PS layer is dewetting, leading to the formation of a PS wetting layer. However, as discussed in the Introduction, the spreading parameter is always negative irrespective of which polymer is on top, and one would also have to conclude that PS cannot wet PMMA. Since the molecular weight has a very small influence on surface energies,[23] the modest differences in molecular weight between our samples and those of Ton-That et al. are not sufficiently effecting the surface and interfacial energies. It is rather the vastly increased viscosity at the higher molecular weight and the lower annealing temperatures that most likely account for the observed differences. To illustrate this conclusion, we prepared 50/50 $PS_{104}/PMMA_{100}$ blends cast from chloroform solution (samples essentially similar to those of Ton-That et al.) and more aggressively annealed these samples. Unannealed, chloroform-cast samples indeed showed a hole morphology (not shown here) identical to that described by Ton-That et al. After annealing for 8 days at 170 °C, however, the chloroform-cast samples exhibit the same type of droplet morphology found in all the toluene-cast samples described here (see Figures 2−4). Chloroform-cast samples annealed for 2 and 4 days exhibited similar droplet morphology (not shown) but had slightly smaller droplets. From a comparison of the droplet size distribution, we conclude that after 8 days of annealing the thermodynamic equilibrium has almost, but not yet, been reached. The surface enrichment of PS observed by Ton-That et al. of samples annealed at 142 °C must be a transient morphology as the PMMA moves to the strongly hydrophilic substrate. Similar nonequilibrium structures of very high molecular polymers annealed at relatively low temperatures have been observed by Morin et al.[21] Since our measurements yield consistently droplets even from samples evolving from vastly different starting morphologies, the morphologies observed are not metastable, kinetically trapped morphologies. Yet, even in the most mobile systems investigated here (prepared from low-M_w materials and annealed at high temperature), true thermodynamic equilibrium has not been reached. The bimodal distribution of large and small droplets suggests that Ostwald ripening is incomplete, and the large droplets should further grow at the expense of the small droplets due to the dependence of chemical potentials on droplet size.

Our results, based on exquisite quantitative compositional surface sensitivity, a symmetric analysis of the spreading parameter, and AFM microscopy, show that the slightly lower surface energy of PS compared to that of PMMA is insufficient for the PS to segregate to the surface and form a wetting layer. Instead, PS and PMMA are phase-separated on the surface. It is only in PS-*b*-PMMA diblock copolymer films that the PS block is always and the PMMA block never at the surface. With block copolymers, the PS block of each copolymer molecule near a surface will segregate to the surface. Yet the two blocks cannot laterally segregate to further lower the system energy by reducing the PS/PMMA interfacial area. Only a blend or bilayer of PS and PMMA can respond with lateral phase separation to lower the system energy.

Acknowledgment. We are grateful for helpful discussions with J. Genzer and A. P. Hitchcock as well as those (numerous) colleagues who motivated this study by supporting the notion that there would be a very thin PS wetting or overlayer on top of PMMA. NEXAFS data were recorded at NSLS U4B. We thank J. Dvorak and D. Arena for experimental support at the beamline. M. Harris and H. Ade were supported by NSF DMR-0071743. G. Appel was supported by DOE DE-FG02-98ER45737.

References and Notes

(1) Tanaka, K.; Takahara, A.; Kajiyama, T. *Macromolecules* **1996**, *29*, 3232.
(2) Ade, H.; Winesett, D. A.; Smith, A. P.; Qu, S.; Ge, S.; Sokolov, J.; Rafailovich, M. *Europhys. Lett.* **1999**, *45*, 526.
(3) Walheim, S.; Boltau, M.; Mlynek, J.; Krausch, G.; Steiner, U. *Macromolecules* **1997**, *30*, 4995.
(4) Winesett, D. A.; Zhu, S.; Sokolov, J.; Rafailovich, M.; Ade, H. *High Perform. Polym.* **2000**, *12*, 599.
(5) Winesett, D. A.; Ade, H.; Sokolov, J.; Rafailovich, M.; Zhu, S. *Polym. Int.* **2000**, *49*, 458.
(6) Zhu, S.; Liu, Y.; Rafailovich, M. H.; Sokolov, J.; Gersappe, D.; Winesett, D. A.; Ade, H. *Nature (London)* **1999**, *400*, 49.
(7) Walheim, S.; Schäffer, E.; Mlynek, J.; Steiner, U. *Nature (London)* **1999**, *283*, 520.
(8) Karim, A.; Slawecki, T. M.; Kumar, S. K.; Douglas, J. F.; Satija, S.; Han, C. C.; Russell, T. P.; Liu, Y.; Overney, R.; Sokolov, J.; Rafailovich, M. H. *Macromolecules* **1998**, *31*, 857.
(9) Affrossman, S.; Henn, G.; O'Neill, S. A.; Pethrick, R. A.; Stamm, M. *Macromolecules* **1996**, *29*, 5010.
(10) Ade, H.; Winesett, D. A.; Smith, A. P.; Anders, S.; Stammler, T.; Heske, C.; Slep, D.; Rafailovich, M. H.; Sokolov, J.; Stöhr, J. *Appl. Phys. Lett.* **1998**, *73*, 3775.
(11) Slep, D.; Asselta, J.; Rafailovich, M. H.; Sokolov, J.; Winesett, D. A.; Smith, A. P.; Ade, H.; Strzhemechny, Y.; Schwarz, S. A.; Sauer, B. B. *Langmuir* **1998**, *14*, 4860.
(12) Ton-That, C.; Shard, A. G.; Daley, R.; Bradley, R. H. *Macromolecules* **2000**, *33*, 8453.
(13) Wu, S. *J. Phys. Chem.* **1970**, *74*, 632.
(14) Stöhr, J. *NEXAFS Spectroscopy*; Springer-Verlag: Berlin, 1992.
(15) http://bama.ua.edu/~gmankey/vacuum/sld017.htm.
(16) Sperling, L. H. *Introduction to Physical Polymer Science*, 2nd ed.; John Wiley and Sons: New York, 1992.
(17) Plazek, D. J.; Ngai, K. L. In *Physical Properties of Polymers Handbook*; Mark, J. E., Ed.; American Institute of Physics: Woodbury, NY, 1996; p 141.
(18) Wyart, F. B.; Martin, P.; Redon, C. *Langmuir* **1993**, *9*, 3682.
(19) Liu, Y.; Russell, T. P.; Samant, M. G.; Stöhr, J.; Brown, H. R.; Cossy-Favre, A.; Diaz, J. *Macromolecules* **1997**, *30*, 7768.
(20) Dhez, O.; Ade, H.; Urquhart, S. *J. Electron Spectrosc. Relat. Phenom.* **2003**, *128*, 85.
(21) Morin, C.; Ikeura-Sekiguchi, H.; Tyliszczak, T.; Cornelius, R.; Brash, J. L.; Hitchcock, A. P.; Scholl, A.; Nolting, F.; Appel, G.; Winesett, A. D.; Kaznacheyev, K.; Ade, H. *J. Electron Spectrosc. Relat. Phenom.* **2001**, *121*, 203.
(22) Reiter, G.; Auroy, P.; Auvray, L. *Macromolecules* **1996**, *29*, 2150.
(23) Wu, S. In *Polymer Handbook*, 3rd ed.; Brandrup, J., Immergut, E. H., Eds.; Wiley: New York, 1986; p VI/411.

MA0257043